Double Line Stimulated Raman Scattering in Benzene

B. Meier, P. Weidner, and A. Penzkofer

Naturwissenschaftliche Fakultät II – Physik, Universität Regensburg, D-8400 Regensburg, Fed. Rep. Germany

Abstract. Simultaneous stimulated Raman scattering at the $992\,\mathrm{cm}^{-1}$ and the $3063\,\mathrm{cm}^{-1}$ line of benzene is observed by mode-locked ruby laser pulse excitation. The double line stimulated Raman scattering is initiated by self-focusing. The influence of small-scale self-focusing, self-phase modulation, and cross-phase modulation on the double line stimulated Raman scattering is discussed. At low pump pulse intensities, before the onset of small-scale self-focusing, the steady-state Raman gain factors of both Raman lines are determined by Raman energy conversion efficiency measurements.

In steady-state stimulated Raman scattering (pump pulse duration $\Delta t_\mathrm{L} \gg$ vibrational dephasing time T_2) only the vibrational line with the highest steady-state Raman gain factor g_S produces an intense Raman Stokes signal (angular Stokes frequency $\omega_\mathrm{S} = \omega_\mathrm{L} - \omega_\mathrm{v}$, with ω_L the angular laser frequency and ω_v the angular vibration frequency) [1–6]. At high pump pulse intensities the stimulated Raman scattering depletes the pump laser energy and higher order Raman Stokes components are generated ($\omega_\mathrm{2S} = \omega_\mathrm{L} - 2\omega_\mathrm{v}$; $\omega_\mathrm{3S} = \omega_\mathrm{L} - 3\omega_\mathrm{v}$; ...), because the first Stokes signal takes over the role of the pump laser and generates the second Stokes line, and so on [7]. The pump pulse depletion prevents the efficient amplification of other spontaneous Raman lines even in the case of very high pump pulse intensities.

Under transient conditions ($\Delta t_\mathrm{L} \lesssim T_2$) the Raman light amplification reduces [3–5, 8–13]. Raman lines with fast dephasing time T_2 gain importance. For $\Delta t_\mathrm{L} \ll T_2$ the Raman line with the highest g_S/T_2 value is amplified preferentially.

The simultaneous stimulated emission of two vibrational Raman lines has been observed in many liquids using nanosecond [14–16] and picosecond [17–20] pump pulses. For the picosecond pulse excitation of methanol the transient stimulated Raman scattering was thought to allow the simultaneous stimulation of the $2837\,\mathrm{cm}^{-1}$ line with the highest g_S value (homogeneous linewidth $\Delta\tilde{v} = 17\,\mathrm{cm}^{-1}$) and the $2942\,\mathrm{cm}^{-1}$ line with the highest g_S/T_2 value ($\Delta\tilde{v} = 34\,\mathrm{cm}^{-1}$) [17]. The importance of spectral broadening of the pump laser and the Raman light for the simultaneous transient Raman amplification of more than one mode was discussed in [20]. The spectral broadening is caused by self-phase modulation [4, 21–29] and cross-phase modulation [30–32].

In this paper we study the simultaneous stimulated Raman scattering of the symmetric ring breathing mode [33–45] at $\tilde{v}_\mathrm{v1} = 992\,\mathrm{cm}^{-1}$ (highest steady-state Raman gain g_S) and of the CH-stretching mode [33, 34, 36, 46–52] at $\tilde{v}_\mathrm{v2} = 3063\,\mathrm{cm}^{-1}$ (shorter dephasing time T_2, highest g_S/T_2 value) of benzene. The benzene samples are excited with picosecond pulses of a passively mode-locked ruby laser [53]. The stimulated Raman scattering is initiated by small-scale self-focusing [4, 21–25, 54–58].

The self-focusing causes self-phase modulation [4, 21–29] of the pump pulse and cross-phase modulation of the Raman signal [30–32, 59, 60]. The pump pulses and the Raman pulses become chirped [61–65]. It will be shown in this paper that the small-scale self-focusing (filament formation, moving self-foci) allows the quasi-steady state double line Raman amplification, and that the different frequency chirping of the pump laser and the Raman signal makes the Raman interaction more transient.

At low pump pulse intensities, before the onset of small-scale self-focusing, the spontaneous Raman scattering signals and the amplified spontaneous Raman signals [42] of both vibrations are detected. Their steady-state Raman gain factors are determined by comparing the experimental Raman conversion efficiencies with numerical simulations. In spontaneous Raman scattering all

Raman lines are visible with scattering peaks proportional to the steady-state Raman gain factors. The spontaneous Raman scattering is independent of the pump laser duration [13].

1. Theoretical Considerations

1.1. Transient Stimulated Raman Scattering

The transient Raman amplification (= amplification of input Raman signal) is described by semiclassical differential equations for the vibrational wave

$$q = 1/2[Q \exp(ik_v z - i\omega_v t) + c.c.]$$

and the electric field strength

$$E = 1/2[E_L \exp(ik_L z - i\omega_L t) + E_S \exp(ik_S z - i\omega_S t) + c.c.].$$

Without pump pulse depletion the equations for the vibrational amplitude Q and the Stokes field amplitude E_S read [3]

$$\frac{\partial Q^*}{\partial t'} + \frac{1}{T_2} Q^* = -i\kappa_Q E_L^* E_S \tag{1}$$

$$\frac{\partial E_S}{\partial z'} = i\kappa_S E_L Q^* \tag{2}$$

where $z' = z$ and $t' = t - n_S z/c_0$ are the travelling wave coordinates. c_0 is the speed of light in vacuum, and n_S is the refractive index at the Stokes frequency $\nu_S = \omega_S/2\pi$. E_L is the electrical field amplitude of the pump laser. The abbreviations κ_Q and κ_S are given by [3]

$$\kappa_Q = \frac{1}{4m_{red}\omega_v} \left[\frac{\partial \alpha}{\partial q}\right] (1 - 2\bar{n}) \tag{3}$$

and

$$\kappa_S = \frac{\omega_S}{4n_S\varepsilon_0 c_0} N \left(\frac{\partial \alpha}{\partial q}\right); \tag{4}$$

m_{red} is the reduced mass of the vibrating structure $[m_{red}(\nu_{v1}) \approx \frac{1}{4} m_{benzene}; \quad m_{red}^{-1}(\nu_{v2}) \approx m_{C_6\text{-ring}}^{-1} + m_H^{-1}]$. $\bar{n} = [\exp(\hbar\omega_v/k_B\vartheta) - 1]^{-1}$ is the thermal population of the vibrational mode (k_B is the Boltzmann constant, and ϑ is the temperature). N is the number density of molecules ($N = \varrho/m_{benzene}$, ϱ density). $\partial\alpha/\partial q$ is the vibrational expansion coefficient of the molecular polarizability [$\alpha = \alpha_0 + (\partial\alpha/\partial q)q + \ldots$]. An isotropic Raman scattering tensor is assumed leading to the scalar form of $\partial\alpha/\partial q$. A homogeneous line broadening is assumed for the vibrational excitation (1).

The relation between $(\partial\alpha/\partial q)$ and the Raman scattering cross-section $(\partial\sigma/\partial\Omega)$ is [3]

$$\frac{d\sigma}{d\Omega} = \frac{\hbar\omega_S^4 n_S}{32\pi^2 m_{red}\varepsilon_0^2 c_0^4 \omega_v n_L} \left(\frac{\partial\alpha}{\partial q}\right)^2, \tag{5}$$

where n_L is the refractive index at the laser frequency.

The transient stimulated Raman scattering (transient amplification of spontaneous Raman light) is simulated by solving (1) and (2) numerically for the initial conditions

of $Q^*(z', -\infty) = 0$ and $E_S(0, t') = (2I_{SN}/n_S\varepsilon_0 c_0)^{1/2}$, where ε_0 is the permittivity of vacuum and I_{SN} is the Stokes noise intensity. After calculation of the Stokes signal $I_S(l) = (n_S\varepsilon_0 c_0/2) |E_S(l)|^2$ the noise input I_{SN} is subtracted.

The Stokes noise intensity I_{SN} [3, 66] for transient interaction is given approximately by

$$I_{SN} \approx \frac{\hbar\omega_S^3 n_S^2}{(2\pi)^3 c_0^2} \Delta\Omega \left[\frac{\pi}{2} \Delta\omega_S + \frac{1}{2} \left(\frac{\pi}{\ln 2}\right)^{1/2} \Delta\omega_L\right]$$

$$= \frac{\hbar\omega_S^3 n_S^2}{8\pi^2 c_0^2 T_2} \Delta\Omega \left[1 + \left(\frac{1}{\pi\ln 2}\right)^{1/2} \frac{\Delta\omega_L}{\Delta\omega_S}\right]$$

$$= I_{SN, st} \left[1 + \frac{1}{2(\pi\ln 2)^{1/2}} T_2\Delta\omega_L\right], \tag{6}$$

where $\Delta\omega_S = 2/T_2 = 2\pi\Delta\nu_S$ is the angular frequency width of the steady-state spontaneous Raman signal, and $\Delta\omega_L = 2\pi\Delta\nu_L$ is the angular frequency width of the pump laser. For Gaussian pulses it is $\Delta\nu_L\Delta t_L = 0.441$ [67]. $\Delta\Omega \approx \pi(\Delta d_L/2l)^2$ is the solid angle of effective stimulated Raman scattering inside the cell (Δd_L is the pump beam diameter and l is the Raman sample length). In the experiments the solid angle of acceptance of the detectors outside the sample $\Delta\Omega_{exp}$ is the set smaller than the external solid angle $n_S^2\Delta\Omega$ of effective stimulated Raman scattering in order to avoid an enlarged collection of spontaneous emission light. $I_{SN, st}$ is the steady-state Stokes noise intensity ($\Delta\omega_L \rightarrow 0$).

The pump pulse shape is assumed to be Gaussian, i.e.

$$I_L = I_{0L} \exp\left(-\frac{t'^2}{t_{0L}^2}\right) \exp\left(-\frac{r^2}{r_{0L}^2}\right) \tag{7}$$

$t_{0L} = \Delta t_L/[2(\ln 2)^{1/2}]$ is half the 1/e-width of the temporal pulse profile, and $r_{0L} = \Delta d_L/[2(\ln 2)^{1/2}]$ is half the 1/e-width of the spatial pulse shape. The relation between the electrical field strength and the intensity of the pump laser is $E_L = (2I_L/n_L\varepsilon_0 c_0)^{1/2}$.

The intensity conversion efficiency of the stimulated Raman light is

$$\eta_I = \frac{I_S(l, t', r)}{I_L(t', r)}. \tag{8}$$

The time integrated conversion efficiency is

$$\eta_{TI} = \frac{\int_{-\infty}^{\infty} I_S(l, t', r)dt'}{\int_{-\infty}^{\infty} I_L(t', r)dt'} = \frac{\int_{-\infty}^{\infty} I_S(l, t', r)dt'}{\pi^{1/2}t_{0L}I_{0L} \exp[-(r/r_{0L})^2]} \tag{9}$$

and the energy conversion efficiency is given by

$$\eta_E = \frac{W_S}{W_L} = \frac{2\int_0^{\infty} r \int_{-\infty}^{\infty} I_S(l, t', r)dt'dr}{\pi^{1/2}r_{0L}^2 t_{0L}I_{0L}}. \tag{10}$$

The energy conversion efficiency within the experimental solid angle $\Delta\Omega_{exp} < n_S^2\Delta\Omega$ is

$$\eta_{E, exp} = \eta_E \frac{\Delta\Omega_{exp}}{n_S^2\Delta\Omega}. \tag{11}$$
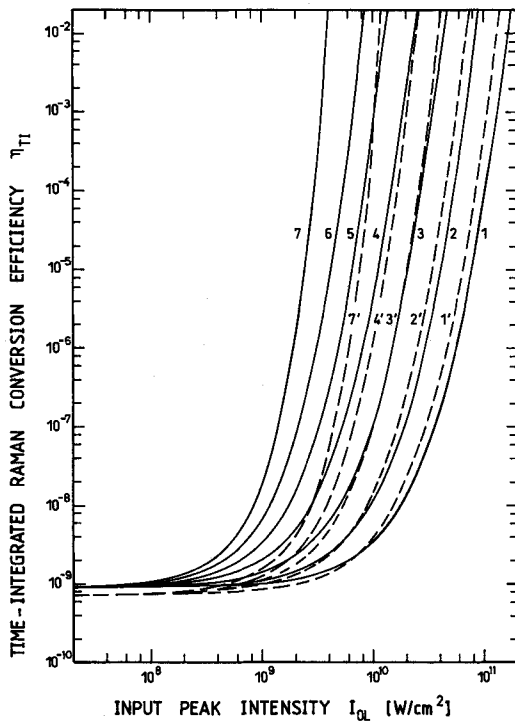
Fig. 1. Time-integrated Raman conversion efficiency η_{TI} versus input peak intensity I_{0L} [Eqs. (1–4, 6, 9)]. Sample length $l=2$ cm. The applied parameters are listed in Table 1. Solid curves belong to 992 cm^{-1} line. Dashed curves belong to 3063 cm^{-1} line of benzene. The pulse durations are (1, 1') $\Delta t_L = 0.5$ ps, (2, 2') 1 ps, (3, 3') 2 ps, (4, 4') 4 ps, (5) 8 ps, (6) 16 ps, (7, 7')∞(steady-state)

Under steady-state conditions $(\Delta t_L \gg T_2, \partial Q^*/\partial t' \ll Q^*/T_2)$ the solution of (1) and (2) leads to

$$I_S(l) = I_{SN,st}[\exp(g_S I_L l) - 1],\qquad(12)$$

where

$$g_S = \frac{4\kappa_Q\kappa_S T_2}{n_L\varepsilon_0 c_0} = \frac{\omega_S T_2}{4n_L n_S \varepsilon_0^2 c_0^2 m_{red}\omega_v} N\left(\frac{\partial\alpha}{\partial q}\right)^2 (1-2\bar{n})$$

$$= \frac{8\pi^2 T_2 c_0^2}{hn_S^3\omega_S^3} N \frac{\partial\sigma}{\partial\Omega}(1-2\bar{n}) = \frac{8\pi c_0^2}{hn_S^3\omega_S^3} N \frac{\partial^2\sigma}{\partial\Omega\partial v}(1-2\bar{n})$$

$$(13)$$

is the steady-state Raman gain factor. The Raman line with the highest value of g_S is amplified preferentially. For the last equality of (13), the relation $\partial^2\sigma/\partial\Omega\partial v = (\pi T_2)\partial\sigma/\partial\Omega$ between the Raman scattering cross-section and the differential Raman scattering cross-section has been used.

The steady-state spontaneous Stokes intensity, $I_{S,sp} = I_{SN,st}g_S I_L l$, is obtained from (12) for $I_L\to 0$. The solution of (1) and (2) for $I_L\to 0$ in the transient case deviates slightly from $I_{S,sp}$ as a result of the approximate line shape factor used in (6) (square brackets). The curves in Fig. 1 are adjusted to the theoretical spontaneous Raman intensity value $I_{S,sp}$ [13].

Under extreme transient conditions, $\Delta t_L \ll T_2$, Eq. (1) simplifies to

$$\frac{\partial}{\partial t'} Q^* = -i\kappa_Q E_L^* E_S \qquad(14)$$

and (2) is given by

$$\frac{\partial E_S(t')}{\partial z'} = \kappa_Q\kappa_S E_L(t') \int_{-\infty}^{t'} E_L^*(t'')E_S(t'')dt'' . \qquad(15)$$

The Raman line with the highest value of $\kappa_Q\kappa_S = (n_L\varepsilon_0 c_0/4)g_S/T_2$ [Eq. (13)] is amplified preferentially.

1.2. Calculations for the 992 cm^{-1} and 3063 cm^{-1} Lines of Benzene

In Fig. 1 time-integrated conversion efficiencies $\eta_{TI}(I_{0L})$ are presented for the 992 cm^{-1} and the 3063 cm^{-1} lines of benzene. Curves are shown for various pump pulse durations. The parameters used in the calculations are collected in Table 1.

The time-integrated efficiency of spontaneous emission within the internal solid angle $\Delta\Omega$ is $\eta_{TI}(I_{0L}\to 0) = I_{SN,st}g_S l$. In the case of steady-state interaction the 992 cm^{-1} line dominates. Under transient conditions the 3063 cm^{-1} line gains importance. For $\Delta t_L < 3$ ps the 3063 cm^{-1} line dominates.

The threshold pump pulse peak intensity, $I_{0L,th}$, necessary for a time-integrated conversion efficiency of
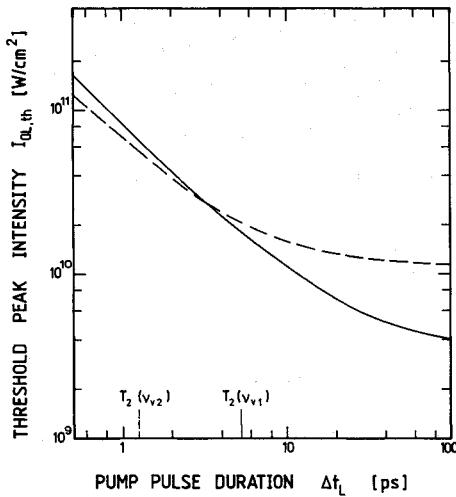
Table 1. Parameters of benzene. Room temperature $(\vartheta = 20°$ C). Laser wavelength $\lambda_L = 694.3$ nm

Parameter		992 cm^{-1}	3063 cm^{-1}	Comments
ω_L [s^{-1}]	2.713×10^{15}			
n_L	1.4982			Ref. [88]
ω_S [s^{-1}]		2.526×10^{15}	2.136×10^{15}	
n_S		1.4960	1.4921	Ref. [88]
ω_v [s^{-1}]		1.869×10^{14}	5.770×10^{14}	
$\bar{n}$		7.73×10^{-3}	2.96×10^{-7}	
ϱ [kg m^{-3}]	879.03			
N [m^{-3}]	6.777×10^{27}			
$\Delta\tilde{v}_S$ [cm^{-1}]		2.04 [81]	8.5 [89]	
T_2 [ps]		5.2	1.25	$T_2 = (\pi c_0 \Delta\tilde{v}_S)^{-1}$
g_S [m W^{-1}]		2.7×10^{-11}	8.8×10^{-12}	Ref. [90], Table 2
$\Delta\Omega$ [sr]	0.016			
$I_{SN,st}$ [W m^{-2}]		1640.7	4105.5	Eq. (6)

Fig. 2. Pump pulse peak intensity $I_{0L,th}$ necessary for time-integrated Raman conversion efficiency of $\eta_{TI} = 0.01$ as a function of the pump pulse duration Δt_L. Solid curve, 992 cm^{-1} line; dashed curve, 3063 cm^{-1} line. Curves are extracted from Fig. 1

$\eta_{TI} = 10^{-2}$ is displayed in Fig. 2 as a function of the pump pulse duration Δt_L. The dephasing times $T_2(v_{v1})$ and $T_2(v_{v2})$ of the two Raman lines are indicated. For $\Delta t_L < 3$ ps the pump pulse threshold intensity is lower for the 3063 cm^{-1} line while for $\Delta t_L > 3$ ps the 992 cm^{-1} line has the lowest threshold intensity.

The Raman gain reduction in the transient case is illustrated in Fig. 3 where the ratio $\eta_{TI}(\Delta t_L/T_2)/\eta_{TI,st}$ is plotted versus $\Delta t_L/T_2$. The laser intensity is chosen so that
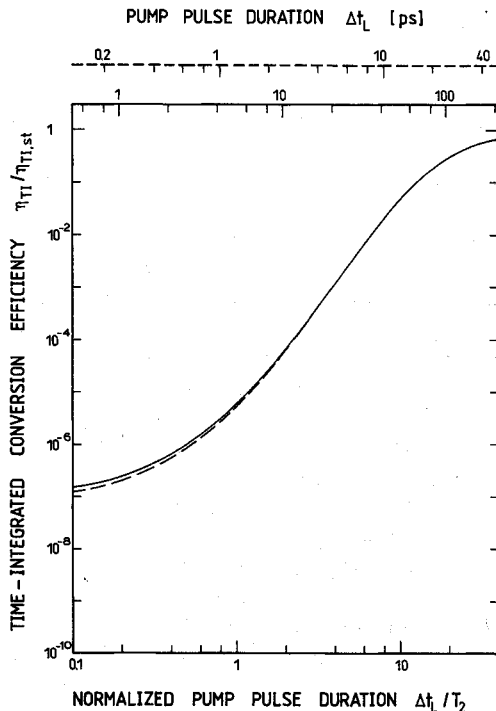

Fig. 3. Transient reduction of the time-integrated stimulated Raman scattering conversion efficiency $\eta_{TI}(\Delta t_L/T_2)/\eta_{TI}(\infty)$ for pump pulse input peak intensities of $I_{0L,th}[\eta_{TI}(\infty) = 0.01]$. Sample length $l = 2$ cm. Solid curve, 992 cm^{-1} line; dashed curve and dashed upper abszissa, 3063 cm^{-1} line. The curves are extracted from Fig. 1

$\eta_{TI,st} = 0.01$. For $\Delta t_L/T_2 > 10$ the steady-state gain is approached, while for $\Delta t_L/T_2 < 0.1$ the ratio approaches the spontaneous emission limit $I_{SN,st}g_s l/0.01$.

1.3. Self-Focusing, Self-Phase-Modulation, and Cross-Phase Modulation

The self-focusing length of whole-beam self-focusing is given by [24, 26, 68, 69]

$$z_{f,wb} = \frac{k_L w_{0L}^2}{2} \frac{1}{\left(\dfrac{P_L}{P_{cr}} - 1\right)^{1/2} + \theta}$$

$$= \frac{2\pi n_L \tilde{v}_L r_{0L}^2}{\left(\dfrac{8\pi^2 n_2 \tilde{v}_L^2 r_{0L}^2 I_L}{c_0 \varepsilon_0} - 1\right)^{1/2} + \theta}, \tag{16}$$

where $w_{0L} = 2^{1/2} r_{0L}$ is the $1/e$ radius of the electrical field strength. $k_L = 2\pi n_L v_L/c_0 = 2\pi n_L \tilde{v}_L$ is the wavenumber of the laser light. $P_L = \pi r_{0L}^2 I_L$ is the laser power and $P_{cr} = c_0 \varepsilon_0/(8\pi n_2 \tilde{v}_L^2)$ [68] is the critical power of whole-beam self-focusing. n_2 is the field coefficient of the nonlinear refractive index. θ is the divergence angle of the incident laser beam.

The whole-beam self-focusing length $z_{f,wb}$ versus input pump pulse peak intensity I_{0L} is shown by the solid curve in Fig. 4 for the situation of

$$r_{0L} = \Delta d_L/[2(\ln 2)^{1/2}] = 1.7 \text{ mm},$$

$$n_2 = 3 \times 10^{-21} \text{ m}^2 \text{V}^{-2} \text{ [70]},$$

and $\theta \approx 0$. The self-focusing length becomes equal to the sample length of $l = 2$ cm used in the experiments at $I_{0L} \approx 7 \times 10^{11}$ W/cm^2. This intensity value is much higher
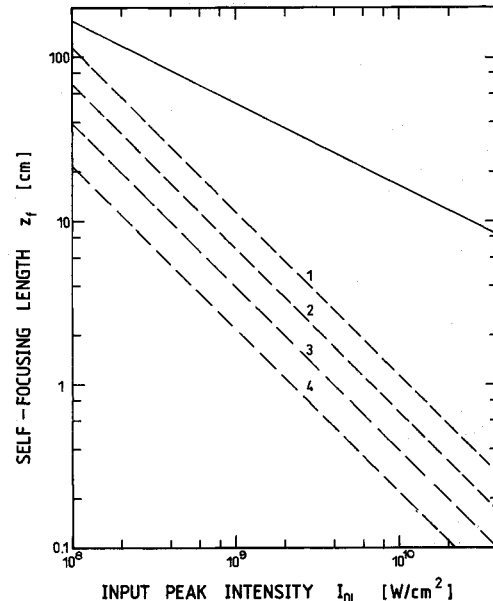

Fig. 4. Self-focusing length versus input peak intensity in benzene. Beam diameter $\Delta d_L = 2.8$ mm (FWHM). Field coefficient of nonlinear refractive index $n_2 = 3 \times 10^{-21}$ mV^{-2}. Solid curve, whole-beam self-focusing. Dashed curves, small-scale self-focusing with modulation depths $\delta_m = 0.01$ (1), 0.1 (2), 0.5 (3), and 1 (4)

than the threshold intensity of $I_{0L,th} \simeq 5 \times 10^9$ W/cm^2 for high conversion efficiency Raman light generation (Fig. 1, $\Delta t_L \approx 30$ ps, 992 cm^{-1} line). The whole-beam self-focusing does not play any role in the stimulated Raman scattering of benzene for laser beam radii $r_{0L} > 0.15$ mm.

A modulation (amplitude irregularity due to the diffraction, dust, refractive index inhomogenities) of the spatial intensity distribution leads to high intensity filament formation by small-scale self-focusing [24, 25, 56–58]. The small-scale self-focusing length $z_{f,ss}$ depends on the modulation spacing and the modulation depth. For optimum modulation spacing $z_{f,ss}$ is given by [25, 58]

$$z_{f,ss} = \frac{n_L^2 c_0 \varepsilon_0}{2\pi \tilde{v}_L n_2 I_L} \ln\left(\frac{3}{\delta_m}\right) \tag{17}$$

where δ_m is the modulation depth of the electrical field strength. $z_{f,ss}(I_{0L})$ curves are included in Fig. 4 for $\delta_m = 0.01$, 0.1, 0.5, and 1. The small-scale self-focusing occurs already at pump laser intensities below the threshold of high efficiency stimulated Raman scattering and therefore the stimulated Raman scattering is enhanced by the small-scale self-focusing.

The self-focusing is accompanied by self-phase modulation [4, 5, 21–25, 71] and cross-phase modulation [30–32] due to an intensity dependent variation of the refractive index. For the pump laser the refractive index variation is [30–32]

$$\Delta n_L = n_2(|E_L|^2 + 2|E_S|^2)/2 \approx \frac{n_2|E_L|^2}{2} \tag{18}$$

and for the Raman Stokes light the refractive index change is

$$\Delta n_S = n_2(|E_S|^2 + 2|E_L|^2)/2 \approx n_2|E_L|^2 . \tag{19}$$

The first terms in the parentheses are responsible for self-phase modulation and the second terms cause the cross-phase modulation. The factor two results from the degeneracy factor in the third-order nonlinear suscepti-bility responsible for the nonlinear refractive index [72, 73]. The last approximations are valid for $I_S \ll I_L$.

The refractive index variations cause frequency chirps which are given by [74]:

$$\omega_L(t') - \omega_{0L} = \frac{\partial \Delta \phi_L}{\partial t'} = -\frac{\partial}{\partial t'} \Delta k_L l$$

$$= -\frac{\omega_{0L} l}{c_0} \frac{\partial}{\partial t'} \Delta n_L \approx -\frac{n_2 \omega_{0L} l}{n_L c_0^2 \varepsilon_0} \frac{\partial I_L}{\partial t'}$$

$$= \frac{2n_2 \omega_{0L} I_{0L} l}{n_L c_0^2 \varepsilon_0 t_{0L}^2} t' \exp(-t'^2/t_{0L}^2) \tag{20}$$

and

$$\omega_S(t') - \omega_{0S} = -\frac{\partial \Delta \phi_S}{\partial t'} = -\frac{\partial}{\partial t'} \Delta k_S l = -\frac{\omega_{0L} l}{c_0} \frac{\partial}{\partial t'} \Delta n_S$$

$$\approx 2\frac{\omega_{0S}}{\omega_{0L}}[\omega_L(t') - \omega_{0L}] . \tag{21}$$

ω_{0L} and ω_{0S} are the non-chirped central frequencies of the laser light and the Raman light. $\Delta \phi_L$ and $\Delta \phi_S$ are the

phase changes, while Δk_L and Δk_S are the changes of the wave vectors of the pump light and the Raman light, respectively. The last equality in (20) valid for temporal Gaussian pulse shapes.

The chirp causes a spectral braodening of

$$\Delta v_{br,L} = \frac{\Delta \omega_{br,L}}{2\pi} = \frac{\omega_{L,max} - \omega_{L,min}}{2\pi}$$

$$\approx \frac{2^{1/2} 2 v_{0L} n_2 I_{0L} l \exp(-1/2)}{n_L c_0^2 \varepsilon_0 t_{0L}} \tag{22}$$

and

$$\Delta v_{br,S} \approx 2\frac{\omega_{0S}}{\omega_{0L}} \Delta v_{br,L} . \tag{23}$$

The last approximation of (22) is valid for Gaussian pulse shapes.

1.4. Quasi-Steady-State Double Line Raman Amplification in Filaments

At high pump laser intensities the dynamics of Stokes and higher order Stokes light generation under quasi-steady-state condition is described by [3,7]

$$\frac{\partial}{\partial z} I_{1S,i} + \gamma(\omega_{1S,i}) I_{1S,i} = g_{S,i}(I_L I_{1S,i} - I_{1S,i} I_{2S,i}) , \tag{24}$$

$$\frac{\partial}{\partial z} I_{2S,i} + \gamma(\omega_{2S,i}) I_{2S,i}$$

$$= g_{S,i} \frac{\omega_{2S,i}}{\omega_{1S,i}}(I_{1S,i} I_{2S,i} - I_{2S,i} I_{3S,i}) , \tag{25}$$

$$\frac{\partial}{\partial z} I_{3S,i} + \gamma(\omega_{3S,i}) I_{3S,i}$$

$$= g_{S,i} \frac{\omega_{3S,i}}{\omega_{1S,i}}(I_{2S,i} I_{3S,i} - I_{3S,i} I_{4S,i}) , \quad \text{etc.} \tag{26}$$

with $i = v1$ or $v2$ and $\omega_{1S,i} - \omega_{2S,i} = \omega_{vi}$ etc. γ is the optical absorption coefficient.

Without self-focusing the first Stokes component with the highest gain factor depletes the pump laser and hinders the efficient amplification of other Raman modes. In the case of quasi-steady-state self-focusing (relaxation time τ_{n2} of nonlinear refractive index coefficient n_2 is short compared to pulse duration Δt_L) self-focusing forms a moving focal point [4, 5, 21–25, 71]. Therefore the laser intensity remains approximately constant over the filament length. Equations (24–26) may be solved under the condition of $I_L = $ constant and $I_{is} \lesssim I_L$ (intensity limited to a maximum value in filament [4, 21–23, 75–80]). The Raman line with the highest gain value is stimulated first, but Raman modes with lower gain are amplified, too. They only need a longer interaction length. The situation of stimulated Raman scattering in moving-foci filaments is illustrated in Fig. 5. The Stokes components of the 992 cm^{-1} mode and of the 3063 cm^{-1} mode build up independently. Between the second and third Stokes component of the 992 cm^{-1} vibration the 3063 cm^{-1} vibration saturates. This calculation is in agreement with experimental observation (Fig. 8 below).
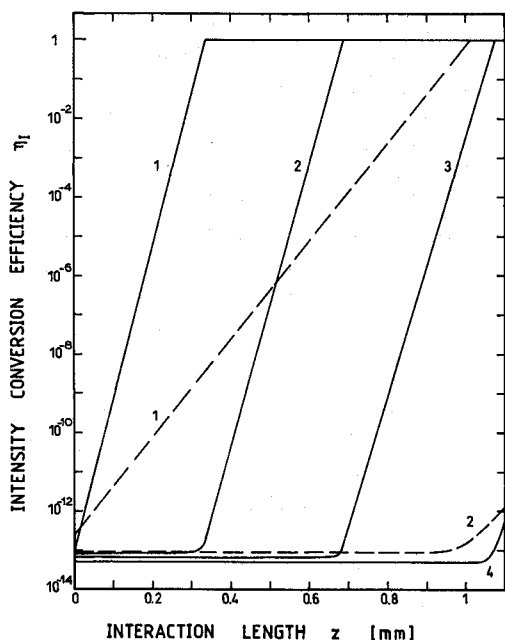
Fig. 5. Simulation of stimulated Raman scattering in a filament without pump pulse depletion and limitation of the Stokes intensities to the pump laser intensity. Laser intensity is set arbitrarily to $I_L = 3 \times 10^{11}$ W/cm^2. Solid curves, 992 cm^{-1} mode. Dashed curves, 3063 cm^{-1} mode. 1: first Stokes, 2: second Stokes, 3: third Stokes, and 4: fourth Stokes component

1.5. Shift to Transient Raman Interaction Due to Chirping

The frequency chirps of the pump laser (20) and of the Raman light (21) are different as long as the intensities of the laser light and the Raman light are not the same. The different chirp shortens the effective interaction time, Δt_{eff}, at a fixed frequency spacing of $\omega_L - \omega_S = \omega_{vi}$ to

$$\Delta t_{eff} \approx \Delta t_L \frac{\Delta v_L}{\Delta v_{br,S} - \Delta v_{br,L} + \Delta v_L} \qquad (27)$$

and Raman scattering becomes more transient. The transient nature of the interaction may be accommodated by setting Δt_{eff} in Fig. 1 instead of Δt_L.

For the passage of a Gaussian ruby laser pulse of $\Delta t_L = 30$ ps through a benzene sample of 2 cm length, a peak intensity of $I_{0L} \gtrsim 7 \times 10^9$ W/cm^2 would be necessary to reduce Δt_L to $\lesssim 3$ ps [see (22, 23, 27) with

$n_2 = 3 \times 10^{-21}$ m^2 V^{-2}] where the 3063 cm^{-1} Raman line dominates over the 992 cm^{-1} Raman line (Fig. 2).

Large chirping (self-phase modulation) is caused by the moving focus dynamics in quasi-steady-state self-focusing [4, 71] and by the pulse shortening and horn-shaping in transient self-focusing [4, 71]. Transient self-focusing occurs for $\Delta t_L \lesssim \tau_{n2}$. For benzene the nonlinear refractive index relaxation time τ_{n2} is given by the molecular reorientation time τ_{or}. Its value is $\tau_{or} \approx 3.1$ ps [81].

2. Experimental Setup

The experimental arrangement for the stimulated Raman scattering studies of the 992 cm^{-1} and the 3063 cm^{-1} lines of benzene and for the determination of the steady-state Raman gain factors of both lines is depicted in Fig. 6. The passively mode-locked ruby laser generates pulses of $\Delta t_L \approx 35$ ps duration at $\lambda_L = 694.3$ nm [53]. Single pulses are separated with a Pockels cell shutter. The pulse energy is increased to the mJ region in a ruby amplifier. The pump pulse peak intensity is detected by energy transmission measurement through either a two-photon absorbing CdS crystal [82] or a saturable absorber [83] (dye DDI in methanol [84], small signal transmission $T_0 = 0.03$, photodetectors PD1 and PD2). The pump pulses are passed through a long-wavelength cutting edge filter before the benzene cell to avoid light input at the Raman frequency which might be due to picosecond light continuum generation [85] in the ruby amplifier [86]. The generated Raman signal in the benzene cell S is collected, filtered, directed to the spectrometer, and detected with a photomultiplier (Valvo type XP 2254 B for 992 cm^{-1} line, RCA type 7102 and Hamamatsu type 636 for 3063 cm^{-1} line). The ruby laser signal transmitted through the benzene sample is measured with photodetector PD3. The wavelength dependent sensitivity of the detection system was calibrated with a tungsten lamp of known color temperature [87].

3. Experimental Results

The energy transmission of the pump laser through the benzene sample (sample length $l = 2$ cm) is displayed in
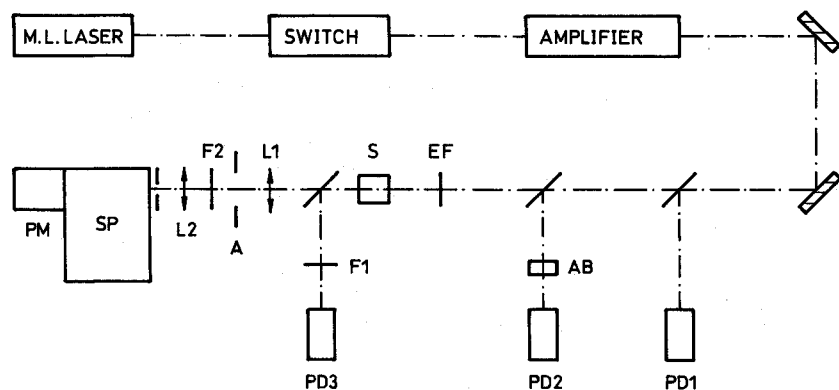

Fig. 6. Experimental setup. PD1–PD3, photodetectors. AB, absorber for peak intensity detection. EF, short-pass edge filter. S, benzene sample. F1, F2, filters. L1, L2, lenses. A, aperture. SP, spectrometer. PM, photomultiplier
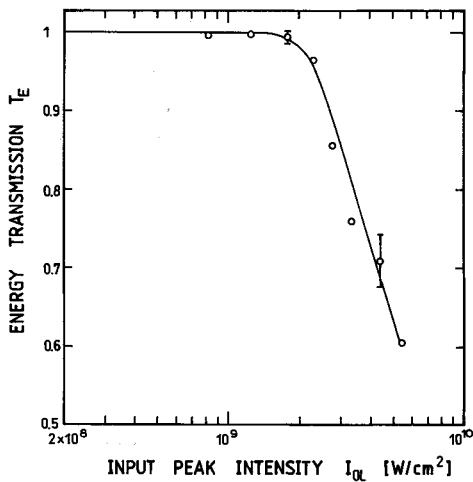
Fig. 7. Energy transmission of picosecond ruby laser pulses ($\Delta t_L \simeq 35$ ps) through benzene. Sample length $l = 2$ cm
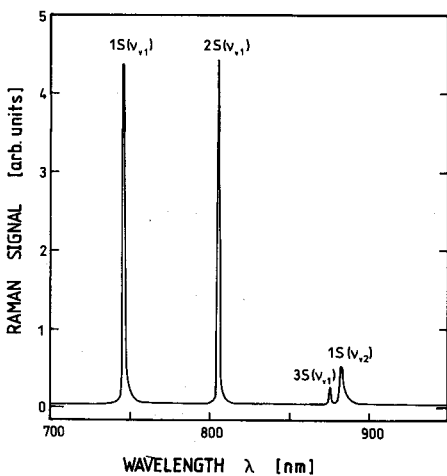

Fig. 8. Stimulated Raman spectrum of benzene. Input pump pulse peak intensity $I_{0L} \approx 8 \times 10^9$ W/cm^2. Sample length $l = 2$ cm. First, second, and third Stokes component of 992 cm^{-1} line, and first Stokes component of 3063 cm^{-1} line are seen. Spectrum is not corrected for spectral sensitivity of detection system [correction would increase the 1S(ν_{v2}) line approximately a factor of two compared to the 1S(ν_{v1}) line]

Fig. 7. The energy transmission reduces above $I_{0L} = 1.7 \times 10^9$ W/cm^2. Above this intensity value strong stimulated Raman scattering is observed.

A stimulated Raman spectrum measured for an input pump pulse peak intensity of $I_{0L} \approx 8 \times 10^9$ W/cm^2 is shown in Fig. 8. The spectrum was recorded with a diode array system behind the spectrometer. The first, second, and third Stokes components of the 992 cm^{-1} Raman line together with the first Stokes component of the 3063 cm^{-1} Raman line are observed.

Detailed Raman spectra of the first Stokes component of the 992 cm^{-1} mode and the 3063 cm^{-1} mode are shown in Fig. 9b, c, respectively. The solid lines represent stimulated Raman spectra for an input pump pulse intensity of $I_{0L} \approx 6.5 \times 10^9$ W/cm^2 (b) and 7.5×10^9 W/cm^2 (c). The dashed curves show the spontaneous Raman spectra [44, 50]. Without self-phase modulation and cross-phase modulation the stimulated spectra should be very narrow compared to the spontaneous Raman spectra. The spectral shape of the ruby laser behind the benzene cell is shown in Fig. 9a for an input peak intensity of $I_{0L} \approx 7 \times 10^9$ W/cm^2. The spectral width of the ruby laser is $\Delta \tilde{\nu}_{br, L} \approx 2.4$ cm^{-1} while the spectral widths of the 992 cm^{-1} and the 3063 cm^{-1} signals are 5 cm^{-1} and 12.5 cm^{-1}, respectively. The bandwidth-limited spectral width of the ruby laser is $\Delta \tilde{\nu}_L \approx 0.441/\Delta t_L c_0 \approx 0.42$ cm^{-1} for a pulse duration of 35 ps. Application of (27) gives an effective stimulated Raman interaction time of Δt_{eff} between 5 ps and 1.4 ps. The Raman amplification of the 992 cm^{-1} line becomes more and more transient and the 3063 cm^{-1} line gains more and more importance.

In the high pump intensity region at $I_{0L} \approx 5 \times 10^9$ W/cm^2 the Raman beam divergence was measured with a diode array system. The full divergence angle was $\Delta \theta \approx 0.2$ rad. Without small-scale self-focusing a divergence angle of $\Delta \theta \leq n_S \Delta d_L/l \approx 0.12$ rad ($\Delta d_L \approx 1.6$ mm) would be expected [74]. The large experimental divergence angle suggests self-focusing.

The filament formation in benzene has been observed by imaging the exit surface of the sample cell to a photographic film. Above 2×10^9 W/cm^2 filament spots have been recorded.
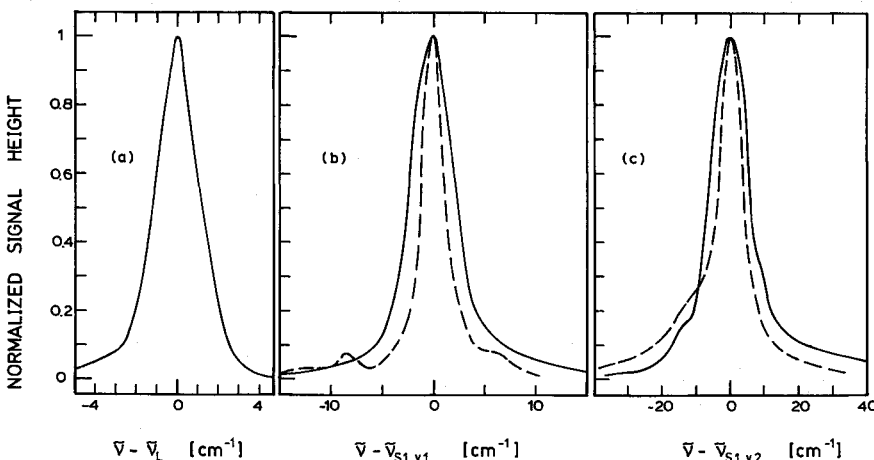

Fig. 9. Spectral shapes of (a) Ruby laser pulse behind benzene sample of 2 cm length. $\Delta t_L \approx 35$ ps, $I_{0L} \approx 7 \times 10^9$ W/cm^2. (b) 992 cm^{-1} Raman line. Solid curve shows stimulated first Stokes component at $I_{0L} \approx 6.5 \times 10^9$ W/cm^2. Dashed curve represents spontaneous Raman spectrum. It is taken from [44]. (c) 3063 cm^{-1} Raman line. Solid curve displays stimulated first Stokes component at $I_{0L} \approx 7.5 \times 10^9$ W/cm^2. Dashed curve is spontaneous Raman spectrum. It is taken from [50]

The experimental Raman conversion efficiencies, $\eta_{E,\exp}$, of the first Stokes components of the 992 cm^{-1} line and the 3063 cm^{-1} line versus input pump pulse peak intensity are shown in Fig. 10. The divergence acceptance angle in these measurements was $\Delta\theta_{\exp}\approx 0.04$ rad ($\Delta\Omega_{\exp}=\frac{1}{4}\pi\Delta\theta_{\exp}^2\approx 0.0013$ sr). The curves are calculated [Eqs. (1–11)]. Up to 9×10^8 W/cm^2 the experimental points are best fitted by steady-state Raman gain factors of

$$g_S(992\ \text{cm}^{-1})=(2.9\pm 0.3)\times 10^{-11}\ \text{m/W}$$

and

$$g_S(3063\ \text{cm}^{-1})=(0.95\pm 0.15)\times 10^{-11}\ \text{m/W}.$$

These g_S values are in good agreement with published data which are collected in Table 2.

Above 10^9 W/cm^2 the experimental points rise more steeply than the theoretical curves because of the onset of filament formation. Above 2×10^9 W/cm^2 the Raman signals begin to saturate because of pump laser depletion (solid angle of stimulated Raman emission is approximately a factor of 10 larger than experimental solid angle of the detection system). At $I_{oL}\approx 6\times 10^9$ W/cm^2 total energy conversion efficiencies of $\eta_E(1S,\nu_{v1})\approx 0.15$ and $\eta_E(1S,\nu_{v2})\approx 0.02$ are measured.
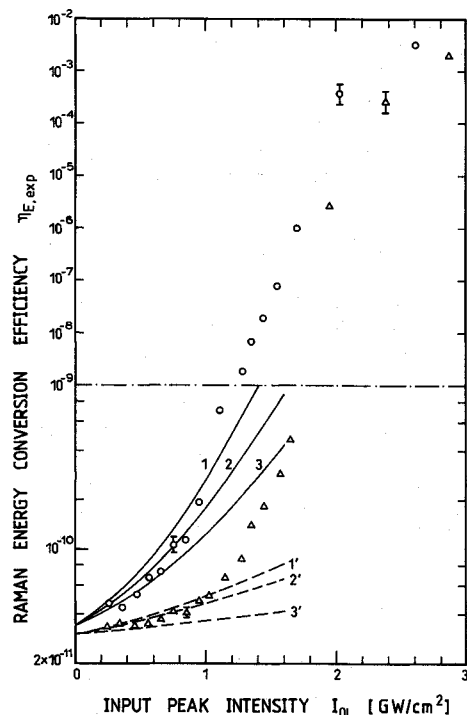
Fig. 10. Raman energy conversion efficiency $\eta_{E,\exp}$ versus input pump pulse peak intensity I_{oL}. Circles belong to 992 cm^{-1} line and triangles belong to 3063 cm^{-1} line. The solid curves are calculated for the 992 cm^{-1} line with (1) $g_S=3.5\times 10^{-11}$ m W^{-1} and $\Delta\Omega_{\exp}=1.05\times 10^{-3}$ sr, (2) $g_S=3.0\times 10^{-11}$ m W^{-1} and $\Delta\Omega_{\exp}=1.23\times 10^{-3}$ sr, (3) $g_S=2.5\times 10^{-11}$ m W^{-1} and $\Delta\Omega_{\exp}=1.48\times 10^{-3}$ sr. The dashed curves are calculated for the 3063 cm^{-1} line with (1') $g_S=1.2\times 10^{-11}$ m W^{-1} and $\Delta\Omega_{\exp}=1.08\times 10^{-3}$ sr, (2') $g_S=1.0\times 10^{-11}$ mW^{-1} and $\Delta\Omega_{\exp}=1.3\times 10^{-3}$ sr, (3') $g_S=5\times 10^{-12}$ mW^{-1} and $\Delta\Omega_{\exp}=2.6\times 10^{-3}$ sr

4. Conclusions

The simultaneous stimulated scattering of two Raman lines of benzene has been studied theoretically and experimentally. Small-scale self-focusing was found to be

Table 2. Raman scattering cross-sections and steady-state Raman gain factors of benzene. λ is excitation wavelength

λ [nm]	$\frac{d\sigma}{d\Omega}(\lambda)$ [cm^2 sr^{-1}]	$\frac{d\sigma}{d\Omega}(694.3\ \text{nm})$[a] [cm^2 sr^{-1}]	$g_S(694.3\ \text{nm})$[b] [cm W^{-1}]	References
$\tilde\nu_{v1}=992$ cm^{-1}				
632.8	6.7×10^{-30}	4.0×10^{-30}	2.6×10^{-9}	[36]
694.3	5.9×10^{-30}	5.9×10^{-30}	3.8×10^{-9}	[35,91]
694.3	9×10^{-30}	9×10^{-30}	5.8×10^{-9}	[92]
488	3.75×10^{-29}	4.95×10^{-30}	3.2×10^{-9}	[38]
694.3	6.6×10^{-30}	6.6×10^{-30}	4.3×10^{-9}	[39]
632.8	8×10^{-30}	4.8×10^{-30}	3.1×10^{-9}	[42,43]
488	3.25×10^{-29}	4.12×10^{-30}	2.7×10^{-9}	[42,43,90]
514.5	2.86×10^{-29}	5.06×10^{-30}	3.3×10^{-9}	[93]
647	7.16×10^{-30}	4.85×10^{-30}	3.1×10^{-9}	[45]
532	1.34×10^{-29}	2.92×10^{-30}	1.9×10^{-9}	[44]
351.4	1.5×10^{-28}	1.57×10^{-30}	1×10^{-9}	[52]
532	$g_S=5\times 10^{-9}$ cm W^{-1}		2.54×10^{-9}[c]	[41]
$\tilde\nu_{v2}=3063$ cm^{-1}				
488	3.29×10^{-29}	3.34×10^{-30}	8.8×10^{-10}	[90]
351.4	1.9×10^{-28}	1.39×10^{-30}	3.7×10^{-10}	[52]

[a] The wavelength dependence of the Raman scattering cross-section is set to $d\sigma/d\Omega\propto\tilde\nu_S^4/(\tilde\nu_a-\tilde\nu)^2$ where $\tilde\nu_a\simeq 39000$ cm^{-1} is an absorption frequency of benzene, and $\tilde\nu=\lambda^{-1}$ is the excitation frequency
[b] Equation (13) with data of Table 1
[c] The wavelength dependence of the Raman gain factor is set to $g_S\propto\tilde\nu_S/(\tilde\nu_a-\tilde\nu)^2$

essential for the low threshold of efficient stimulated Raman scattering and the stimulation of two vibrational modes. The moving focal point filament formation feeds in pump laser energy to the filament channel over a prolonged time and allows the continuous build-up of Raman lines of lower Raman gain value. The self-phase modulation and cross-phase modulation accompanying the self-focusing cause different frequency chirps of the pump and the Raman light and shorten the effective interaction time of stimulated Raman amplification. As a result the stimulated Raman scattering becomes more transient and the Raman line with the highest g_S/T_2 value (highest Raman scattering cross-section $\partial\sigma/\partial\Omega$) gains importance compared to the line with the highest g_S value (highest differential Raman scattering cross-section $\partial^2\sigma/\partial\Omega\partial\nu$).

References

1. N. Bloembergen: Am. J. Phys. **35**, 989 (1967)
2. W. Kaiser, M. Maier: In *Laser Handbook*, Vol. 2, ed. by F.T. Arecchi, E.O. Schulz-Dubois (North-Holland, Amsterdam 1972) Chap. E2
3. A. Penzkofer, A. Laubereau, W. Kaiser: Prog. Quantum Electron. **6**, 55 (1979)
4. Y.R. Shen: *The Principles of Nonlinear Optics* (Wiley, New York 1984)
5. M. Schubert, B. Wilhelmi: *Nonlinear Optics and Quantum Electronics* (Wiley, New York 1986)
6. M. Maier: Appl. Phys. **11**, 209 (1976)
7. D. von der Linde, M. Maier, W. Kaiser: Phys. Rev. **178**, 11 (1969)
8. A. Laubereau, W. Kaiser: Rev. Mod. Phys. **50**, 3607 (1978)
9. C.S. Wang: In *Quantum Electronics*, Vol. 1, ed. by H. Rabin, C.L. Tang (Academic Press, New York 1975) p. 447
10. R.L. Carman, F. Shimizu, C.S. Wang, N. Bloembergen: Phys. Rev. A **2**, 60 (1970)
11. W.H. Lowdermilk, G.I. Kachen: Appl. Phys. Lett. **27**, 133 (1975)
12. S.A. Akhmanov, K.N. Drabovich, A.P. Suchorukov, A.S. Chirkin: Sov. Phys. JETP **32**, 266 (1971)
13. N. Bloembergen, M.J. Colles, J. Reintjes, C.S. Wang: Ind. J. Pure Appl. Phys. **9**, 874 (1974)
14. G. Eckhardt, R.W. Hellwarth, F.J. McClung, S.E. Schwarz, D. Weiner, E.J. Woodbury: Phys. Rev. Lett. **9**, 455 (1962)
15. M.D. Martin, E.L. Thomas: IEEE J. QE-**2**, 196 (1966)
16. M. Golombok, F.J. Bergin, D.B. Pye: J. Raman Spectrosc. **20**, 805 (1989)
17. R.L. Carman, M.E. Mack, F. Shimizu, N. Bloembergen: Phys. Rev. Lett. **23**, 1327 (1969)
18. O. Rahn, M. Maier, W. Kaiser: Opt. Commun. **1**, 109 (1969)
19. T. Kobayashi: Opt. Commun. **28**, 147 (1979)
20. P.A. Cornelius, C.B. Harris: Opt. Lett. **6**, 129 (1981)
21. S.A. Akhmanov, R.V. Khokhlov, A.P. Sukhorukov: In *Laser-Handbook*, Vol. II, ed. by F.T. Arecchi, E.O. Schulz-Dubois (North-Holland, Amsterdam) Chap. E3
22. Y.R. Shen: Prog. Quantum Electron. **4**, 1 (1975)
23. J.H. Marburger: Prog. Quantum Electron. **4**, 35 (1975)
24. J.F. Reintjes: *Nonlinear Optical Parametric Processes in Liquids and Gases* (Academic Press, Orlando 1984)
25. W. Koechner: *Solid State Laser Engineering*, 2nd edn., Springer Ser. Opt. Sci., Vol. 1 (Springer, Berlin, Heidelberg 1988)
26. N. Bloembergen, P. Lallemand: Phys. Rev. Lett. **16**, 81 (1966)
27. R.G. Brewer: Phys. Rev. Lett. **19**, 8 (1967)
28. F. Shimizu: Phys. Rev. Lett. **19**, 1097 (1967)
29. T.K. Gustafson, J.P.E. Taran, H.A. Haus, J.R. Lifsitz, P.L. Kelley: Phys. Rev. **177**, 306 (1969)
30. J.I. Gersten, R.R. Alfano, M. Belic: Phys. Rev. A **21**, 1222 (1980)
31. G.P. Agrawal: In *The Supercontinuum Laser Source*, ed. by R.R. Alfano (Springer, New York 1989) p. 91
32. P.L. Baldeck, P.P. Ho, R.R. Alfano: In *The Supercontinuum Laser Source*, ed. by R.R. Alfano (Springer, New York 1989) p. 117
33. N. Herzfeld, C.K. Ingold, H.G. Poole: J. Chem. Soc. **1946**, 316
34. F.R. Dollish, W.G. Fateley, F.F. Bentley: *Characteristic Raman Frequencies of Organic Compounds* (Wiley, New York 1974) Chap. 13
35. F.J. McClung, D. Weiner: J. Opt. Soc. Am. **54**, 641 (1964)
36. T.C. Damen, R.C.C. Leite, S.P.S. Porto: Phys. Rev. Lett. **14**, 9 (1965)
37. W.R.L. Clements, B.P. Stoicheff: Appl. Phys. Lett. **12**, 246 (1968)
38. J.G. Skinner, W.G. Nilsen: J. Opt. Soc. Am. **58**, 113 (1968)
39. J.B. Grun, A.K. McQuillan, B.P. Stoicheff: Phys. Rev. **180**, 61 (1969)
40. M.J. Colles: Opt. Commun. **1**, 169 (1969)
41. F. Aussenegg, V. Deserno: Opt. Commun. **2**, 295 (1970)
42. Y. Kato, H. Takuma: J. Opt. Soc. Am. **61**, 347 (1971)
43. Y. Kato, H. Takuma: J. Chem. Phys. **54**, 5398 (1971)
44. A. Owyoung, P.S. Peercy: J. Appl. Phys. **48**, 674 (1977)
45. M.O. Trulson, R.A. Mathies: J. Chem. Phys. **84**, 2068 (1986)
46. A.F. Bunkin, A.S. Galumyan, Kh.A. Zumanov, D.V. Maltsev, K.O. Surskii: Opt. Spectrosc. **60**, 593 (1986)
47. C.K.N. Patel, A.C. Tam: Appl. Phys. Lett. **34**, 760 (1979)
48. A. Fendt, S.F. Fischer, W. Kaiser: Chem. Phys. Lett. **82**, 350 (1981)
49. C. Kolmeder, W. Zinth, W. Kaiser: Chem. Phys. Lett. **91**, 323 (1982)
50. W. Proffitt, S.P.S. Porto: J. Opt. Soc. Am. **63**, 77 (1973)
51. J.P. Stromman, K. Nakamoto: *Laboratory Raman Spectroscopy* (Wiley, New York 1984)
52. Y. Prior, H. Vogt: Phys. Rev. B **19**, 5388 (1979)
53. P. Sperber, A. Penzkofer: Opt. Commun. **54**, 160 (1985)
54. J. Gazengel, G. Rivoire: Optica Acta **26**, 483 (1979)
55. A.N. Arbatskaya: In *Stimulated Raman Scattering*, ed. by N.G. Basov, Proceedings of the Lebedev Physics Institute, Vol. 99 (Consultants Bureau, New York 1982) p. 1
56. V.L. Bespalov, V.I. Talanov: JETP Lett. **3**, 307 (1966)
57. A.J. Campilo, S.L. Shapiro, B.R. Suydam: Appl. Phys. Lett. **23**, 628 (1973)
58. A.J. Campilo, S.L. Shapiro, B.R. Suydam: Appl. Phys. Lett. **24**, 178 (1974)
59. D. Schadt, B. Jaskorzynska: J. Opt. Soc. Am. B **4**, 856 (1987)
60. A. Höök, D. Anderson, M. Lisak: J. Opt. Soc. Am. B **6**, 1851 (1989)
61. E.B. Treacy: Phys. Lett. **28A**, 34 (1968)
62. A. Laubereau, D. von der Linde: Z. Naturforsch. **25a**, 1626 (1970)
63. D. Grischkowsky, A.C. Balant: Appl. Phys. Lett. **41**, 1 (1982)
64. B. Nikolaus, D. Grischkowsky: Appl. Phys. Lett. **43**, 228 (1983)
65. M.D. Duncan, R. Mahon, L.L. Tankersley, J. Reintjes: J. Opt. Soc. Am. B **5**, 37 (1988)
66. A. Einstein: Phys. Z. **18**, 121 (1917)
67. E.P. Ippen, C.V. Shank: In *Ultrashort Light Pulses*, ed. by S.L. Shapiro, Topics Appl. Phys. **18** (Springer, Berlin, Heidelberg 1977) p. 83
68. P.W. Milonni, J.H. Eberly: *Lasers* (Wiley, New York 1988) Chap. 7
69. A. Yariv: *Quantum Electronics*, 2nd edn. (Wiley, New York 1975)
70. B. Meier, A. Penzkofer: Appl. Phys. B **49**, 513 (1989)
71. Y.R. Shen, G.-Z. Yang: In *The Supercontinuum Laser Source*, ed. by R.R. Alfano (Springer, New York 1989) p. 1
72. P.N. Butcher: *Nonlinear Optical Phenomena*, Bulletin 200, Engineering Experiment Station, Ohio State University (Columbus, Ohio 1965)

73. R.W. Minck, R.W. Terhune, C.C. Wang: Appl. Opt. **5**, 1595 (1966)
74. A. Penzkofer: Prog. Quantum Electron. **12**, 291 (1988)
75. M. Maier, W. Kaiser, J.A. Giordmaine: Phys. Rev. **177**, 580 (1969)
76. O. Rahn, M. Maier: Phys. Rev. Lett. **29**, 558 (1972)
77. E. Yablonovitch, N. Bloembergen: Phys. Rev. Lett. **29**, 907 (1972)
78. N. Bloembergen: Opt. Commun. **8**, 288 (1973)
79. M.M.T. Loy, Y.R. Shen: IEEE J. QE-9, 409 (1973)
80. F. Shimizu: IBM J. Res. Dev. **17**, 286 (1973)
81. D. Samios, T. Dorfmüller: Chem. Phys. Lett. **117**, 165 (1985)
82. W. Blau, A. Penzkofer: Opt. Commun. **36**, 419 (1981)
83. A. Penzkofer, D. von der Linde, A. Laubereau: Opt. Commun. **4**, 377 (1972)
84. W. Blau, R. Reber, A. Penzkofer: Opt. Commun. **43**, 210 (1982)
85. A. Penzkofer, W. Kaiser: Opt. Quantum Electron. **9**, 315 (1977)
86. P. Sperber, W. Spangler, B. Meier, A. Penzkofer: Opt. Quantum Electron. **20**, 395 (1988)
87. W. Bäumler, A. Penzkofer: Chem. Phys. **140**, 75 (1990)
88. Landoldt-Börnstein, 6th edition, edited by K.A. Hellwege, A.M. Hellwege (Springer, Berlin, Heidelberg 1962) Vol. 2, Part 8
89. W. Seifert, K.L. Oehme, G. Rudakoff, W. Hölzer, W. Carius, O. Schröter: Chem. Phys. Lett. **105**, 645 (1984)
90. J.R. Nestor, E.R. Lippincott: J. Raman Spectrosc. **1**, 305 (1973)
91. G. Eckhardt, W.G. Wagner: J. Mol. Spectrosc. **19**, 407 (1966)
92. G. Bret, M. Denariez, F. Gires, G. Mayer, M. Paillette: J. Chem. Phys. (Paris) **64**, 197 (1967)
93. N. Abe, M. Wakayama, M. Ito: J. Raman Spectrosc. **6**, 38 (1977)